

Electrochemical deprotonation of phosphate on stainless steel

S. Da Silva, R. Basséguy, A. Bergel*

Laboratoire de Génie Chimique, UMR-CNRS 5503, Basso Cambo, 5 rue Paulin Talabot, BP 1301, 31106 Toulouse, France

Received 19 September 2003; received in revised form 28 January 2004; accepted 12 April 2004

Abstract

Voltammetric experiments performed in phosphate buffer at constant pH 8.0 on platinum and stainless steel revealed clear reduction currents, which were correlated to the concentrations of phosphate. On the basis of the reactions proposed previously, a model was elaborated, assuming that both H_2PO_4^- and HPO_4^{2-} underwent cathodic deprotonation, and including the acid–base equilibriums. A kinetic model was derived by analogy with the equations generally used for hydrogen evolution. Numerical fitting of the experimental data confirmed that the phosphate species may act as an efficient catalyst of hydrogen evolution via electrochemical deprotonation. This reaction may introduce an unexpected reversible pathway of hydrogen formation in the mechanisms of anaerobic corrosion. The possible new insights offered by the electrochemical deprotonation of phosphate in microbially influenced corrosion was finally discussed.

Keywords: Steel; Phosphate; Modelling; Hydrogen evolution; Microbially influenced corrosion

1. Introduction

A few studies have observed that phosphate ions H_2PO_4^- may lead to unexpected electrochemical reactions on platinum, and it has been proposed in early nineteenth that phosphate may undergo an electrochemical deprotonation on platinum electrode [1–3]. To our knowledge, these works did not get an important feedback, even if an abnormal behaviour have commonly been remarked in phosphate-containing solutions around the cathodic potential values where proton reduction occurs. A probable so-called “reduction of phosphate” ions has sometimes been evoked to give a name to this anomalous behaviour [4,5], but the theory seems not to have been developed from the early proposal.

The present study firstly confirmed the previous experimental results obtained on platinum, and showed that phosphate ions exhibited the same electrochemical behaviour on stainless steel. The purpose of the work was then to elaborate a theoretical model on the basis of the reactions that have been proposed already. The set of reactions was completed

with the acid–base equilibriums, a kinetic model was derived from, and it was numerically solved. The experimental results obtained on stainless steel and the theoretical conclusions drawn from the model gave new elements to interpret some still unexplained data in the field of microbially influenced corrosion (MIC). The discussion focused the new insights that the electrochemical deprotonation of phosphate may offer into anaerobic MIC of steels.

2. Materials and methods

Dipotassium hydrogenophosphate, potassium dihydrogenophosphate, nitric acid (65 wt.%), hydrofluoric acid (40 wt.%), and potassium chloride were purchased from Prolabo.

The platinum electrode was a 90% Pt–10% Ir 2 mm diameter disk (Engelhard Comptoir Lyon-Alemand-Louyot, France) inserted in a PTFE tip mounted in a rotating electrode system (Copenhagen Radiometer). Before each experiment, platinum electrode was polished with a 6 μm diamond particle paste (Lam Plan) and cleaned with distilled water in ultrasonic bath.

* Corresponding author. Tel.: +33 5 34 61 52 48; fax: +33 5 34 61 52 53.
E-mail address: alain.bergel@ensiacet.fr (A. Bergel).

Stainless steel electrode was a 316L grid, 29.5 meshes/cm woven with a 0.14 mm-diameter wire (Gantois, France). Its composition was: 16.5–18.0 wt.% Cr, 10.0–12.0 wt.% Ni, ≤ 0.030 wt.% C, ≤ 0.015 wt.% S, ≤ 2.0 wt.% Mn, ≤ 0.75 wt.% Si, ≤ 0.040 wt.% P, ≤ 2.0 – 2.5 wt.% Mo, (maximum) 0.035 wt.% N, bulk Fe. Twenty-four hours before each experiment, the working electrode was pre-treated by 10 min immersion in a nitric acid (20 vol.%)—hydrofluoric acid (2 vol.%) solution, followed by 10 min in a nitric acid (20 vol.%) solution. The auxiliary electrode was a platinum grid (Engelhard Comptoir Lyon-Alemand-Louyot, France). The reference electrode, a saturated calomel electrode (SCE), was connected to the cell with a Luggin capillary filled with the standard solution.

Experiments with the platinum rotating disk were performed in a 50 ml classic cell (Metrohm, Switzerland). The 316L stainless steel grids were inserted between two glass slides, which were maintained thanks to Araldite[®] glue, to form thin spectro-electrochemical cells (TSEC). The volume of these cells was of the order of 100 μ l, with a grid electrode of approximately 3 cm² geometrical surface and 8 cm² real surface areas. All experiments were monitored with a Schlumberger Solartron 1286 electrochemical interface.

3. Experimental results

3.1. Platinum electrode

Current–potential curves were recorded on a platinum rotating disk (diameter 2 mm, rotating speed 1000 rad/min) dipping in a classic electrochemical cell, which contained phosphate buffer at different concentrations: 25, 50, 75 and 100 mM, and KCl 0.1 M. The pH was always controlled strictly at the same value 8.0 for each solution. The solution was deoxygenated by 15-min argon bubbling before experi-

Table 1

Current values measured at -1.00 V/SCE from current–potential curves performed in de-oxygenated potassium phosphate solutions at pH 8.0 containing 0.1 M of KCl

Concentration (mM)	Current (mA)
25	0.33
50	0.62
75	0.89
100	1.30

Working electrode was a 2 mm platinum disk electrode (rotating speed 1000 rad/min). Scan rate was 20 mV s⁻¹.

ment. Before curve recording a 5-min electrolysis was performed at -0.50 V/SCE to reduce the platinum oxides. The potential was then scanned at 20 mV s⁻¹ from -0.50 to -1.30 V/SCE (Fig. 1). The different concentrations of phosphate gave clear diffusion-limited currents in the potential range from approximately -0.80 to -1.00 V/SCE. The current values measured at -1.00 V/SCE (Table 1) were directly proportional to the concentration of phosphate.

These results are consistent with the experiments reported by Takahera et al. [3]. The voltammograms recorded at 100 mV s⁻¹ with immobile platinum electrodes immersed in Na₂HPO₄ solutions pH 7.4 showed clear reduction peaks around -0.7 V versus Ag/AgCl. The peak currents were proportional to Na₂HPO₄ concentrations in the range from 10 to 50 mM.

3.2. 316L stainless steel grid electrode

The TSEC was constituted of a 316L stainless steel grid electrode tightly maintained between two glass slides (Fig. 2). The cell thickness, which corresponded to space between the slides, was in the range from 0.239 to 0.386 mm. Only the bottom of the cell was open and was dipped in a flat beaker, which contained the platinum auxiliary electrode and the

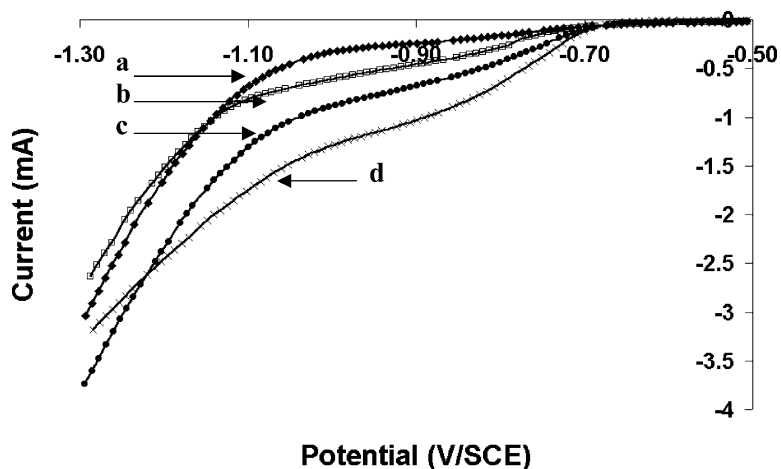


Fig. 1. Current–potential curves performed in de-oxygenated potassium phosphate solutions at pH 8.0 containing 0.1 M of KCl. Working electrode was a 2 mm platinum disk electrode (rotating speed 1000 rad/min). Scan rate was 20 mV s⁻¹. Before curve recording, a 5-min electrolysis was performed at -0.50 V/SCE for each phosphate concentration: (a) 25 mM, (b) 50 mM, (c) 75 mM and (d) 100 mM of potassium phosphate.

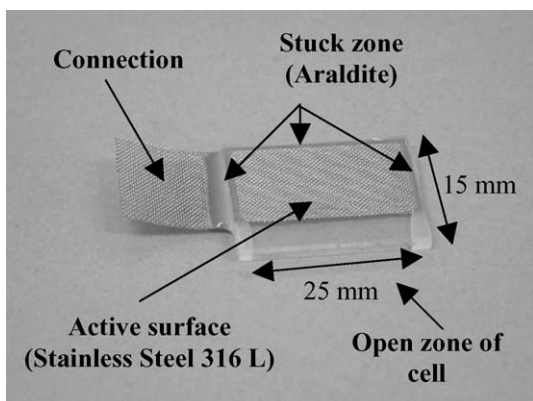


Fig. 2. The thin spectro-electrochemical cell (TSE).

end of the Luggin capillary connected to the saturated calomel reference electrode (SCE). This kind of cell allowed UV-vis spectrophotometric measurements to be performed through the glass slides and the grid electrode, but this possibility was not used here. The cells were filled with phosphate solutions at different concentrations, pH 8.0, containing 0.1 M KCl. As classically done, a preliminary 15-min electrolysis was performed at -0.65 V/SCE to reduce the dissolved oxygen and to reduce the oxides on the electrode surface [6]. The potential was then scanned at the chosen rate from -0.65 to -1.50 V/SCE.

The current-potential curves recorded at 1 and 10 mV s^{-1} are reported in Figs. 3 and 4, respectively. The phosphate concentrations were 5, 12.5, 25 and 50 mM. For each curve, the pH value was identically equal to 8.0. A particular attention was focused on the electrode surface state. Stainless steel electrodes were made up from the same stainless steel grid and pre-treated thoroughly in the same conditions in order to obtain the more suitable results. Previous works [6,7] using chrono-amperometry technique showed that the electrode surface states after the electro-reduction of oxides (at -0.65 V/SCE during 15 min) were totally identical. Following results were obtained from

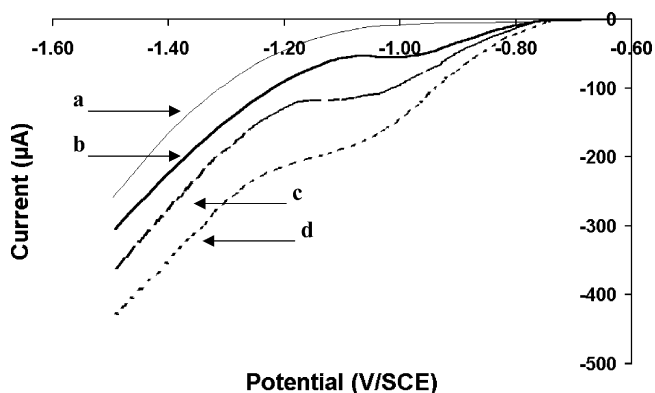


Fig. 3. Current-potential curve performed in a potassium phosphate solution at pH 8.0 containing 0.1 M of KCl. Working electrode was a 316L stainless steel assembled in a TSE. Scan rate was 1 mV s^{-1} . Before curve recording, a 15-min electrolysis was performed at -0.65 V/SCE: (a) 5 mM, (b) 12.5 mM, (c) 25 mM and (d) 50 mM of potassium phosphate.

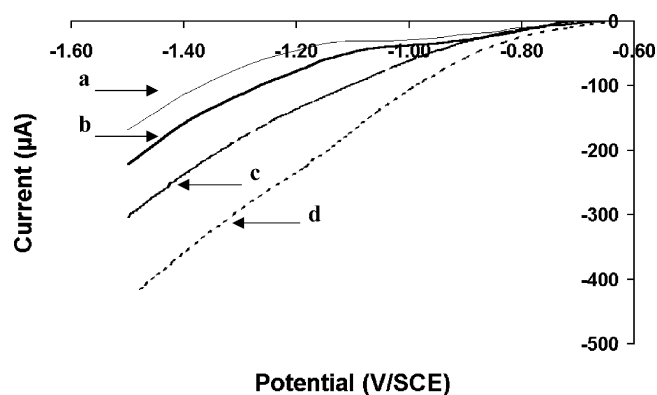


Fig. 4. Current-potential curve performed in a potassium phosphate solution at pH 8.0 containing 0.1 M of KCl. Working electrode was a 316L stainless steel assembled in a TSE. Scan rate was 10 mV s^{-1} . Before curve recording, a 15-min electrolysis was performed at -0.65 V/SCE: (a) 5 mM, (b) 12.5 mM, (c) 25 mM and (d) 50 mM of potassium phosphate.

experiments performed with the same treatment conditions and presented with deviations. As on the platinum electrode a current plateau was observed at 1 mV s^{-1} , with values directly correlated to the concentration of phosphate.

One of the main advantages of the TSEC is that they can be reasonably modelled according to the thin layer assumption [8]. Actually, it was preferred here not to use the term of “thin layer cell”, because it would not be rigorously exact. For a purely reversible electrochemical reaction, an electrochemical cell acts as a thin layer cell if the potential scan rate is lower than a limit imposed by the characteristics of the cell [9]:

$$|\text{“scan rate”}| < \frac{RTD\pi^2}{3nFL^2} \log\left(\frac{1-\varepsilon}{1+\varepsilon}\right) \quad (1)$$

where R is the gas constant, T temperature, D diffusion coefficient of the electroactive species, n number of electron exchanged, F Faraday’s constant, ε error on the measure of the peak current, and L characteristic length of the electrode. Here, the thickness of the cell was imposed by the thickness of the grid, because each glass slide was exactly applied against the grid. This thickness was consequently not representative of the diffusion phenomenon. It was preferred to choose as characteristic length the average radius of the mesh ($105 \mu\text{m}$), which was more relevant for diffusion. Using a quite common value for the diffusion coefficient ($D = 10^{-9} \text{ m}^2 \text{ s}^{-1}$), and assuming that one electron is exchanged ($n = 1$), Eq. (1) gave a maximal deviation ε from the thin layer cell assumption of 15%. Theoretically, a value around 9% for ε remains quite acceptable [10]. As a consequence, the TSEC that was used here was not a rigorous thin layer cell, but it may be reasonably agreed that it does not excessively deviated from a thin layer cell behaviour for potential scan of 1 mV s^{-1} .

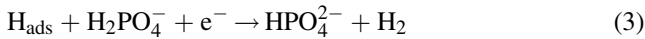
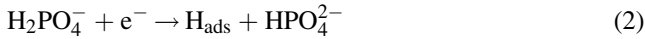
Two different curve shapes are encountered in thin layer cells: either exponential-shaped curves due to a pure electrochemical kinetics limitation step, or peak-shaped curves

due to limitation by depletion of the electroactive species in the small volume of the cell. At 10 mV s^{-1} the curves may be interpreted as two successive exponential-shaped phenomena, which may correspond to the phosphate deprotonation and water reduction respectively. On the contrary, at 1 mV s^{-1} the shape of the experimental current–potential curves did not correspond to the shapes commonly expected for elementary reactions in thin layer cells. No peak-shaped curve was observed, as it could be expected. On the other hand, the plateau currents, which appeared in the potential range from -1.00 to -1.20 V/SCE , cannot be attributed to diffusion-limited currents, which can absolutely not occur in a real thin layer cells, and that could not so obviously appear here, with respect to the rather low deviation of only 15%. A more complex kinetic model has to be elaborated.

4. Kinetic model

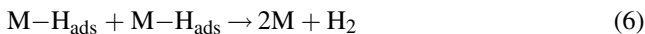
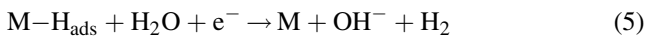
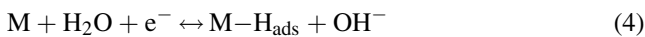
4.1. Equations

O’Neil et al. [2] and then Takehara et al. [3] assumed that phosphate ions interact with an electron to give an adsorbed hydrogen atom H_{ads} , which can further react with another phosphate ion:



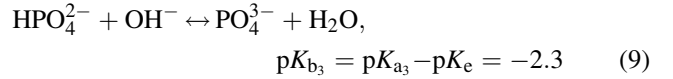
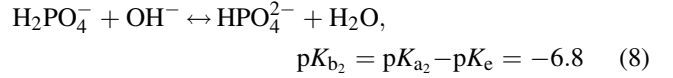
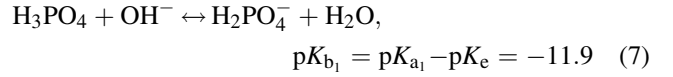
They proposed this reaction to be responsible of the reduction peaks they obtained on the platinum electrode. In this scheme, the electrochemical reaction does not modify the phosphate oxidation state, but only the proton extracted from the phosphate ion is reduced. We consequently preferred to call this reaction “electrochemical deprotonation” of phosphate, rather than “reduction” of phosphate, which may be confusing.

A kinetic model was elaborated here on the basis of the equations that are widely used for hydrogen evolution [11–13]. At pH 8.0, the reduction of the protons can be neglected, and hydrogen evolution is generally represented by a set of three equations:

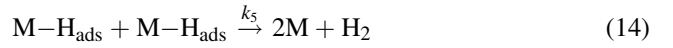
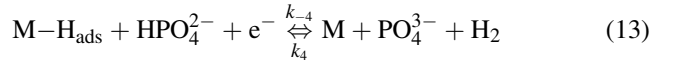
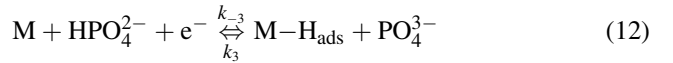
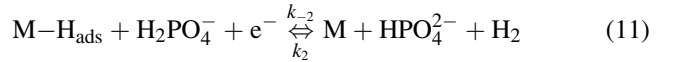
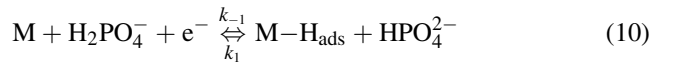


where M represents a site on the electrode surface where water can adsorb, and $\text{M}-\text{H}_{\text{ads}}$ the same surface site occupied by adsorbed hydrogen. The first mono-electronic reduction of water that results in H adsorption (Volmer reaction) is followed by two irreversible parallel reactions, namely the electrochemical (Heyrovsky reaction) and/or chemical (Tafel reaction) desorption of hydrogen.

According to the $\text{p}K_{\text{b}}$ values of phosphoric acid [14]:



the concentration of H_3PO_4 can be neglected at pH 8.0. Both species H_2PO_4^- and HPO_4^{2-} are assumed to deprotonate on the electrode surface as suggested by Takehara et al. [3]. By analogy to hydrogen evolution, we proposed the following kinetics model for the electrochemical deprotonation of phosphate:



The reaction rates r_i were written assuming Langmuirian adsorption behaviour as follows:

$$r_1 = k_1^0 \exp(-\alpha_1 f \eta) (1-\theta) [\text{H}_2\text{PO}_4^-] \quad (15)$$

$$r_{-1} = k_{-1}^0 \exp((1-\alpha_1) f \eta) \theta [\text{HPO}_4^{2-}] \quad (16)$$

$$r_2 = k_2^0 \exp(-\alpha_2 f \eta) \theta [\text{H}_2\text{PO}_4^-] \quad (17)$$

$$r_{-2} = k_{-2}^0 \exp((1-\alpha_2) f \eta) (1-\theta) [\text{HPO}_4^{2-}] [\text{H}_2] \quad (18)$$

$$r_3 = k_3^0 \exp(-\alpha_3 f \eta) (1-\theta) [\text{HPO}_4^{2-}] \quad (19)$$

$$r_{-3} = k_{-3}^0 \exp((1-\alpha_3) f \eta) \theta [\text{PO}_4^{3-}] \quad (20)$$

$$r_4 = k_4^0 \exp(-\alpha_4 f \eta) \theta [\text{HPO}_4^{2-}] \quad (21)$$

$$r_{-4} = k_{-4}^0 \exp((1-\alpha_4) f \eta) (1-\theta) [\text{PO}_4^{3-}] [\text{H}_2] \quad (22)$$

$$r_5 = k_5 \theta^2 \quad (23)$$

where k_i^0 are rate constants, α_i are symmetry factors, η is the overpotential, θ is the degree of coverage of the electrode surface by atomic hydrogen, and $f = F/RT$. For simplicity, it was assumed that the symmetry factors are equal to 0.5. The overpotential was expressed with respect to the initial value of the potential ($E_{\text{init}} = -0.65 \text{ V/SCE}$):

$$\eta = E - E_{\text{init}} = \text{“scan rate”} \cdot t \quad (24)$$

where “scan rate” is the potential scan rate (negative for a reduction scan), and t the time. Consequently the values of the kinetic constants k_i^0 correspond to the initial potential E_{init} . Reaction rates are in units of flux ($\text{mol dm}^{-2} \text{ s}^{-1}$).

The assumption was made that the electrochemical reaction of phosphates on stainless steel is slower than the acid–base equilibria. Consequently, the concentrations of the different phosphate species were supposed to be controlled by the acid–base equilibria (8) and (9):

$$K_{b2} = \frac{[\text{HPO}_4^{2-}]}{[\text{H}_2\text{PO}_4^-][\text{OH}^-]} \quad (25)$$

$$K_{b3} = \frac{[\text{PO}_4^{3-}]}{[\text{HPO}_4^{2-}][\text{OH}^-]} \quad (26)$$

$[\text{H}_3\text{PO}_4]$ being neglected at pH 8.0, conservation of phosphate species led to:

$$[\text{P}]^0 = [\text{H}_2\text{PO}_4^-] + [\text{HPO}_4^{2-}] + [\text{PO}_4^{3-}] \quad (27)$$

These equations allowed the different phosphate species concentrations to be straightforwardly expressed as a function of the concentration of hydroxide ions $[\text{OH}^-]$:

$$[\text{H}_2\text{PO}_4^-] = \frac{[\text{P}]^0}{1 + K_{b2}[\text{OH}^-] + K_{b2}K_{b3}[\text{OH}^-]^2} \quad (28)$$

$$[\text{HPO}_4^{2-}] = \frac{K_{b2}[\text{OH}^-][\text{P}]^0}{1 + K_{b2}[\text{OH}^-] + K_{b2}K_{b3}[\text{OH}^-]^2} \quad (29)$$

$$[\text{PO}_4^{3-}] = \frac{K_{b2}K_{b3}[\text{OH}^-]^2[\text{P}]^0}{1 + K_{b2}[\text{OH}^-] + K_{b2}K_{b3}[\text{OH}^-]^2} \quad (30)$$

The degree of coverage θ was extracted from the transient mass balance on the electrode surface:

$$\frac{d\theta}{dt} = \frac{F}{\sigma} (r_1 - r_{-1} - r_2 + r_{-2} + r_3 - r_{-3} - r_4 + r_{-4} - 2r_5) \quad (31)$$

where σ is the charge required for a monolayer coverage per dm^2 by atomic hydrogen.

It was assumed that the phosphate acid–base equilibria were very fast as compared to the electrochemical reactions. Consequently, the reactions of H_2PO_4^- deprotonation (reactions (10) and (11)), which transform H_2PO_4^- to HPO_4^{2-} , actually result in the production of OH^- via the fast back transformation of HPO_4^{2-} to H_2PO_4^- due to the acid–base equilibrium (reaction (8)). Reactions (12) and (13) of HPO_4^{2-} deprotonation can be processed in the same way. In other words, a pseudo-stationary state was assumed on the phosphate species, as schematised on Fig. 5. According to the thin layer assumption, the concentration of each species is considered uniform in the cell [9]. For the lowest scan rate (1 mV s^{-1}), this assumption can reasonably be used. In this case the transient mass balances are simply expressed by classic differential equations instead of the partial derivative equations that would be required if concentration gradients had to be taken into consideration.

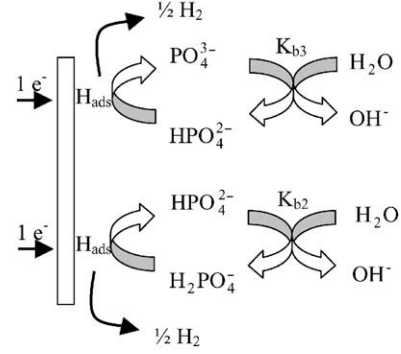


Fig. 5. Scheme of the electrochemical deprotonation of phosphate on stainless steel in a pseudo-stationary state.

The transient mass balance relative to the hydroxide ions was thus:

$$V \frac{d[\text{OH}^-]}{dt} = A(r_1 - r_{-1} + r_2 - r_{-2} + r_3 - r_{-3} + r_4 - r_{-4}) \quad (32)$$

where V is the volume of the cell, and A the electrode surface area.

Finally, the current was given by the expression:

$$I = FA(r_1 - r_{-1} + r_2 - r_{-2} + r_3 - r_{-3} + r_4 - r_{-4}) \quad (33)$$

The differential equations (31) and (32) were solved numerically by a Runge–Kutta technique. At each time step, the current was calculated with Eq. (33), and the concentration of the phosphate species were calculated with Eqs. (28)–(30) and introduced into Eqs. (31) and (32) for the further time step. As final result the model gave the concentration of each species and the current as a function of time. The current–time curves were further transformed into current–potential curves.

The initial time ($t = 0$) corresponded to the beginning of the potential scan, at the end of the preliminary 15-min electrolysis. Initially $[\text{OH}^-] = 10^{-6} \text{ M}$, and the value of $[\text{P}]^0$ led to the initial phosphate concentrations through Eqs. (28) and (29). The current was considered equal to zero, which led to:

$$0 = r_1 - r_{-1} + r_2 - r_{-2} + r_3 - r_{-3} + r_4 - r_{-4} \quad (34)$$

The initial value of the degree of coverage θ_{init} was extracted from this last equation:

$$\theta_{\text{init}} = \frac{k_1^0[\text{P}]^0}{(k_1^0 - k_2^0)[\text{P}]^0} + k_{-1}^0[\text{HPO}_4^{2-}]_{\text{init}} \quad (35)$$

The values of the different geometrical, operating and physicochemical parameters used in the model are reported in Table 2. The only unknown parameters are the kinetic constants k_1^0 , k_{-1}^0 , k_2^0 , k_{-2}^0 , k_3^0 , k_{-3}^0 , k_4^0 , k_{-4}^0 , k_5 , and σ the charge required for a mono-layer coverage by hydrogen. In the absence of previous kinetic study dealing with phosphate

Table 2

Values of different geometrical, operating and physicochemical parameters used in the model

Constants and parameters	Symbol	Values
Real electrode surface (dm ²)	A	8×10^{-2}
Symmetry factors	$\alpha_i \beta_i$	0.5
Initial potential (V/SCE)	E_i	-0.65
Temperature (K)	T	298
Volume (dm ³)	V	100×10^{-6}
Equilibrium acid–base constant	K_{b_2}	6.2×10^6
	K_{b_3}	2.2×10^2
Charge (C dm ⁻²)	σ	0.01

deprotonation, it was chosen to take equal the values of the kinetic constants relative to H_2PO_4^- and HPO_4^{2-} . The only unknown parameters, which remained to be adjusted, were consequently: k_1^0 , k_{-1}^0 , k_2^0 , k_{-2}^0 , k_5 , and σ .

4.2. Theoretical results

The values of the kinetic constants and σ were adjusted by a trial and error approach. The experimental current–potential curves recorded at the slower scan rate (1 mV s^{-1}) were chosen for fitting to remain as close as possible to the thin layer hypothesis. The theoretical current–potential curves obtained are presented in Fig. 6 (bold lines) for three different phosphate concentrations 12.5, 25 and 50 mM, and the optimal parameter values are reported in Table 3. The parameter values found in the literature for water hydrogen evolution are also reported in Table 3. The experimental conditions used in the study dealing with hydrogen evolution (0.2 M [NaOH], mild steel electrode) [12,13] were obviously very different from the conditions used here. Moreover, the forms of the kinetics rate expression are different. For water hydrogen evolution, the kinetic equa-

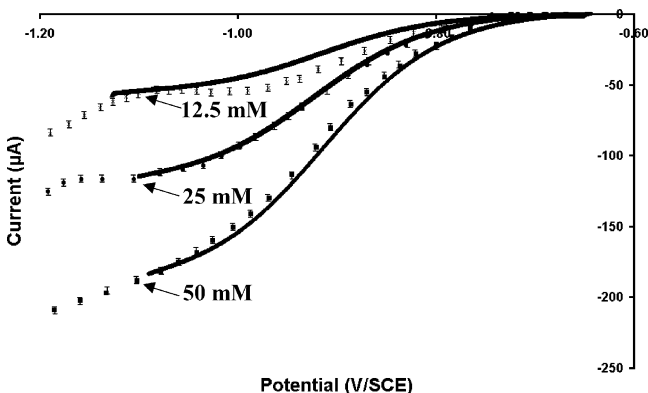


Fig. 6. Theoretical current–potential curves (bold line) obtained for the optimum values reported in Table 3. Comparison with the experimental current–potential curves (dotted lines) obtained in potassium phosphate solutions at pH 8.0 containing 0.1 M of KCl. Working electrode was a 316L stainless steel assembled in a TSCE. Scan rate was 1 mV s^{-1} .

Table 3

Constant rates comparison derived from the phosphate deprotonation model with constant values proposed in water hydrogen evolution

Phosphate deprotonation		Water hydrogen evolution	
k_1^0 (dm s ⁻¹)	5×10^{-9}	$k_{1\text{water}}^0$ (dm s ⁻¹)	1.22×10^{-12}
k_{-1}^0 (dm s ⁻¹)	10^{-7}	$k_{-1\text{water}}^0$ (dm s ⁻¹)	1.25×10^{-8}
k_2^0 (dm s ⁻¹)	1.5×10^{-12}	$k_{2\text{water}}^0$ (dm s ⁻¹)	1.02×10^{-12}
k_{-2}^0 (dm ⁴ mol ⁻¹ s ⁻¹)	10^{-9}	n.d.	n.d.
k_5 (mol dm ⁻² s ⁻¹)	1.2×10^{-8a}	k_5 (mol dm ⁻² s ⁻¹)	1.2×10^{-8}
	7.5×10^{-9b}		
	3.5×10^{-9c}		

Scan rate was 1 mV s^{-1} . n.d.: not determined.

^a 12.5 mM of phosphate.

^b 25 mM of phosphate.

^c 50 mM of phosphate.

tions relative to reactions (4)–(6) were:

$$r_{1\text{water}} = k_{1\text{water}}^0 \exp(-\alpha_1 f \eta) (1 - \theta) \quad (36)$$

$$r_{-1\text{water}} = k_{-1\text{water}}^0 \exp((1 - \alpha_1) f \eta) \theta \quad (37)$$

$$r_{2\text{water}} = k_{2\text{water}}^0 \exp(-\alpha_2 f \eta) \theta \quad (38)$$

$$r_5 = k_5 \theta^2 \quad (23)$$

The concentrations of H_2O and OH^- do not appear, because they are formally included in the kinetic constants k_{water}^0 , expressed in dm s^{-1} , instead of $\text{mol dm}^{-2} \text{ s}^{-1}$. The values of $k_{1\text{water}}^0$ and $k_{2\text{water}}^0$ from the literature were consequently divided by the water concentration (55.6 M in standard conditions), and $k_{-1\text{water}}^0$ by OH^- concentration (Table 3) to be pertinently compared with the values of k_1^0 , k_{-1}^0 and k_2^0 that were obtained here. Logically, k_1^0 was higher than $k_{-1\text{water}}^0$, according to the higher electro-activity of phosphate. The other parameters were of the same order of magnitude. Actually, this comparison has only a limited meaning, because of the different mechanisms and operating conditions, but it confirms that the values obtained here by numerical adjustment physically make sense. Unfortunately it was necessary to slightly modify the value of k_5 with respect to phosphate concentration that may represent a weakness of the model.

The model gave the evolution of the concentration of each species (Fig. 7) and of the hydrogen coverage ratio θ (Fig. 8) as a function of potential for 50 mM phosphate. The hydrogen coverage ratio varied from a value close to zero to an almost complete coverage for potential more negative than -1.00 V/SCE . Comparing the variation of the concentrations of H_2PO_4^- and HPO_4^{2-} shows that H_2PO_4^- was consumed preferentially to HPO_4^{2-} ; HPO_4^{2-} started to be consumed only when H_2PO_4^- was almost completely consumed. This behaviour results from the acid–base equilibria on the one hand, and the values of the electro-chemical kinetics on the other hand. It must be kept in mind that for seek of simplicity, the kinetic constant relative to

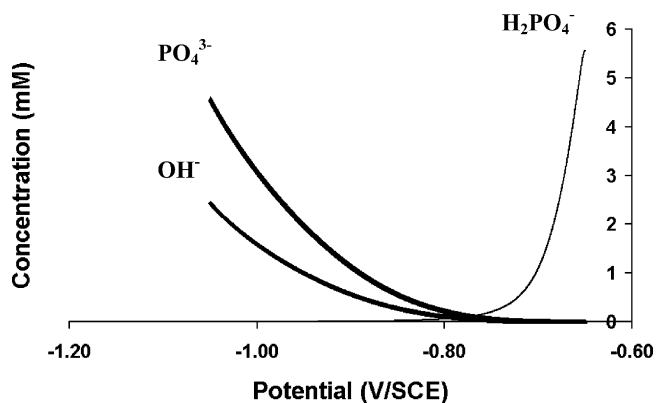


Fig. 7. Theoretical evolution of concentration of species involved in the model as a function of potential for optimum values. Theoretical curves were calculated from a 50 mM potassium phosphate solution at pH 8.0. Scan rate was 1 mV s^{-1} .

both phosphate species were taken equal. The validity of this assumption has to be checked before deriving definitive conclusions on this item.

Evolution of hydrogen concentration is reported in Fig. 9 for three different scan rates and 50 mM phosphate concentration. Phosphate deprotonation obviously produced a great quantity of hydrogen, which exceeded the hydrogen solubility of 0.8 mM [14] (also reported in Fig. 9) from potential values of -0.93 V/SCE for the 1 mV s^{-1} scan rate. The model perfectly confirmed that hydrogen bubbles should appear at the end of the potential scan, as it was experimentally observed. TSEC were well suited to detect gas bubbles as soon as they appear, because they remain entrapped in the grid electrode thanks to the small cell thickness. Nevertheless, strictly speaking, the model should no longer be valid when hydrogen was evolving, for two reasons:

- the real hydrogen concentration never reached values higher than the solubility value, the model consequently used an overestimated value of dissolved hydrogen con-

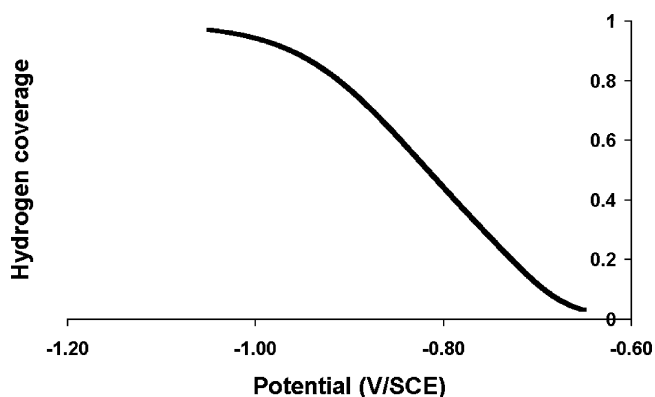


Fig. 8. Theoretical evolution of hydrogen coverage ratio (θ) as a function of potential for a 50 mM potassium phosphate solution at pH 8.0 (optimum values). Scan rate was 1 mV s^{-1} .

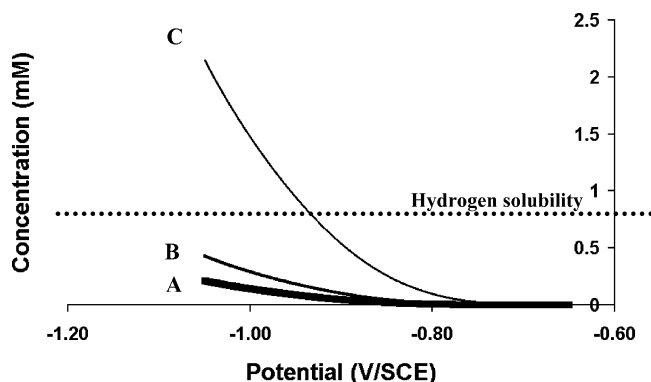


Fig. 9. Theoretical evolution of hydrogen concentration as a function of potential for a 50 mM potassium phosphate solution at pH 8.0 (optimum values). Scan rates were: (A) 10 mV s^{-1} , (B) 5 mV s^{-1} , (C) 1 mV s^{-1} .

centration in the rate expressions r_{-2} and r_{-4} at the most negative potentials;

- occurrence of hydrogen bubbles, decreased the active surface area of the electrode, and this effect was not taken into account in the model.

The model indicated that increasing the scan rate resulted in delaying the occurrence of hydrogen bubbles, and consequently enlarging the potential range where the model was valid. On the contrary, the thin layer hypothesis used to write the mass balance equation (32) is valid only at low scan rates. The TSEC would drastically deviate from a thin layer behaviour for higher scan rates. These two contradictory phenomena led to choose the current–potential curves recorded at 1 mV s^{-1} to perform the numerical fitting. This choice was only a compromise, and the model has still to be improved, including for instance the effect of hydrogen evolution, to get a wider validity in range of potential. The usefulness of thin cells might be discussed. Actually, the thin layer hypothesis leads to simplified equations for transient phenomena (differential equations instead of partial derivatives), and it avoids using diffusion coefficients, as it would be necessary with a rotating disk electrode for instance. Moreover, it was easy to work under anaerobic conditions, after reduction of dissolved oxygen by a preliminary electrolysis. On the contrary, the mesh and thickness of the stainless steel grids used here were not thin enough to allow using the cells at higher scan rates. Improving the theoretical results should require to refine the experimental cells.

The new results obtained here can be summarized as:

- (1) the experimental results obtained by Takehara et al. on platinum were confirmed;
- (2) similar electrochemical deprotonation of phosphate was observed on 316L stainless steel;
- (3) completing the electrochemical deprotonation reaction with the acid–base equilibriums revealed that phosphate

species act as catalyst of water reduction into hydrogen (Fig. 5);

- (4) a kinetic model was proposed on the basis of the classic equations established for hydrogen evolution; the theoretical curves well matched the experimental data;
- (5) the experimental results and the model showed that a significant quantity of molecular hydrogen was produced by this mechanism;
- (6) the model suggested that the global reaction may be considered as reversible.

5. Discussion

The results presented here led to suggest an innovative analysis of several experiments reported in the literature dealing with the role of the cathodic formation of hydrogen in the anaerobic MIC of steels. It is agreed that anaerobic corrosion of steels is driven by the spontaneous cathodic reduction of water/proton into hydrogen. In some cases, the presence of deposited Sulfate Reducing Bacteria (SRB), which commonly growth in anaerobic environment (marine sediments e.g.), drastically enhance the corrosion of carbon steels and other materials. Different assumptions have been proposed to explain how SRB can enhance corrosion: the production of H₂S by these bacteria [15] and the subsequent formation of iron sulfide deposits [16–18] are the most cited.

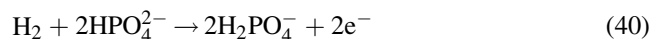
The involvement of the enzyme hydrogenase, which is produced by some SRB, has been often suspected and discussed [6,7,19–22]. Bryant and Laishley described exciting experiments performed with pure hydrogenase [23]. Steel coupons were immersed in a bottle that only contained a phosphate solution, while hydrogenase and methyl viologen used as electron acceptor were in a second bottle; the two liquid phases were totally separated, the bottles were connected only through the common gas phase. No contact was possible between enzyme and carbon steel, but the presence of hydrogenase in the second bottle increased the corrosion rate of 19%. The blue colour observed in the second bottle confirmed the occurrence of the hydrogenase-catalysed reduction of methyl viologen:



These results were very intriguing because they could only be interpreted through the consumption of molecular hydrogen from the gas phase. How the consumption of hydrogen in the second bottle can affect the corrosion that occurs in the first bottle? Considering that the overall reaction of spontaneous hydrogen evolution is a strictly irreversible process, the depletion of the molecular hydrogen in the gas phase cannot have any effect on the hydrogen evolution rate, and cannot explain the increase of corrosion rate. To our knowledge, no fundamental explanation of this experimental observation has been given yet.

Bryant and Laishley remarked that corrosion occurred only when a compound, such as phosphate, was present in the first bottle. The capability of phosphate species to catalyse water reduction into hydrogen, which was demonstrated here, might give a new element to the discussion. Phosphate deprotonation may be a supplementary cathodic reaction that can enhance the anodic metal dissolution. Moreover, if the deprotonation reaction is reversible, as assumed here, the consumption of hydrogen in the gas phase would explain the increase of the corrosion rates, because of the equilibrium shift. Deprotonation of phosphate might be the equilibrated reaction that has been lacking until now in order to explain the influence of hydrogen consumption on MIC.

The reversibility of the deprotonation reaction is obviously a key point to support this assumption. The model was built according to a reversible scheme, and fitting the experimental data did not reject this assumption. Moreover, Takehara et al. [3] have demonstrated experimentally this reversibility by recording voltammograms in the presence of added hydrogen. They have suggested a possible back reaction:



Nevertheless, because of the importance of possible applications in the domain of corrosion further work is still required to confirm the reversibility of the electrochemical deprotonation of phosphate, and to validate the hypothesis suggested here. Further analytical work is also required to better determine the value of the numerous kinetic constants, and to avoid modification of k_5 as a function of phosphate concentration.

Finally, it should be noticed that most corrosion studies that have dealt with hydrogenase have been conducted in phosphate buffer. The involvement of the phosphate-catalysed production of hydrogen has never been taken into consideration in these works. The mechanisms proposed here might consequently modify a part of the theoretical conclusions that have been driven until now.

6. Conclusions

The electrochemical deprotonation of phosphate was investigated, following the previous suggestion of O'Neil et al. The occurrence of this reaction on 316L stainless steel was revealed. A complete set of equations, which included the different acid–base equilibriums, revealed that phosphate species act as catalyst of water reduction into hydrogen. The experimental data and the theoretical model showed that a significant quantity of molecular hydrogen was produced by this mechanism, and the model suggested that the global reaction may be considered as reversible. These results are suspected to give a new insights in the mechanism of anaerobic MIC. Particularly, they might give

for the first time to our knowledge a theoretical explanation of the two-bottle experiments, which were reported more than 20 years ago. The kinetic model remains to be improved, the reversibility of the mechanisms being the key point to be emphasised.

Acknowledgements

The authors wish to thank 6T-MIC Ingénierie to its contribution in the soft conception of the numerical resolution.

References

- [1] S.U.M. Khan, G. Liu, *J. Electroanal. Chem.* 270 (1989) 237.
- [2] P. O'Neil, F. Busi, V. Concialini, O. Tubertini, *J. Electroanal. Chem.* 284 (1990) 59.
- [3] K. Takehara, I. Ide, T. Nakazato, N. Yoza, *J. Electroanal. Chem.* 293 (1990) 285.
- [4] M. Ciszowska, Z. Stojek, J.G. Osteryoung, *J. Electroanal. Chem.* 398 (1995) 49.
- [5] S. Daniele, I. Lavagnini, M.A. Baldo, F. Magno, *Anal. Chem.* 70 (1998) 285.
- [6] S. Da Silva, R. Basséguy, A. Bergel, *J. Electroanal. Chem.* 561 (2004) 93.
- [7] S. Da Silva, R. Basséguy, A. Bergel, *Bioelectrochemistry* 56 (2002) 77.
- [8] R. Devaux, A. Bergel, M. Comtat, *AIChE* 41 (1995) 1944.
- [9] A.J. Bard, L.R. Faulkner, *Electrochemical Methods*, Wiley, New York, 2001.
- [10] A.T. Hubbard, *J. Electroanal. Chem. Interfacial Electrochem.* 22 (1969) 165.
- [11] A. Lasia, A. Rami, *J. Electroanal. Chem.* 294 (1990) 123.
- [12] S.Y. Quian, B.E. Conway, G. Jerkiewicz, *J. Chem. Soc., Faraday Trans. 94* (1998) 2945.
- [13] S.Y. Quian, B.E. Conway, G. Jerkiewicz, *PCCP, Phys. Chem. Chem. Phys.* 1 (1999) 2805.
- [14] *CRC Handbook of Chemistry and Physics*, CRC Press, New York, 1996.
- [15] J.A. Costello, *South Afr. J. Sci.* 70 (1974) 202.
- [16] J.N. Wanklyn, C.J.P. Spruit, *Nature* 169 (1952) 928.
- [17] R.C. Salvarezza, H. Videla, *Corrosion* 36 (1980) 550.
- [18] R.C. Salvarezza, H. Videla, A.J. Arvia, *Corros. Sci.* 23 (1983) 717.
- [19] R.D. Bryant, E.J. Laishley, *Can. J. Microbiol.* 36 (1990) 259.
- [20] R. Cord-Ruwisch, F. Widdel, *Appl. Microbiol. Biotechnol.* 25 (1986) 169.
- [21] S. Daumas, Y. Massiani, J. Crousier, *Corros. Sci.* 28 (1988) 1041.
- [22] F. Van Ommen Kloeke, R.D. Bryant, E.J. Laishley, *Anaerobe* 1 (1995) 351.
- [23] R.D. Bryant, L. Laishley, *Appl. Microbiol. Biotechnol.* 38 (1993) 824.